

NEAR-INFRARED EMISSION LINES IN STARBURST GALAXIES AT $0.5 < z < 0.9$: DISCOVERY OF A MERGER SEQUENCE OF EXTREME OBSCURATIONS

A. CALABRÒ¹, E. DADDI¹, P. CASSATA², M. ONODERA^{3,4}, R. GOBAT⁵, A. PUGLISI¹, S. JIN^{1,6}, D. LIU⁷, R. AMORÍN^{8,9}, N. ARIMOTO¹⁰, M. BOQUIEN¹¹, R. CARRARO¹², D. ELBAZ¹, E. IBAR¹², S. JUNEAU¹³, F. MANNUCCI¹⁴, H. MÉNDEZ HERNÁNDEZ¹², E. OLIVA¹⁴, G. RODIGHIERO², F. VALENTINO^{15,16}, AND A. ZANELLA¹⁷

1, CEA, IRFU, DAp, AIM, Université Paris-Saclay, Université Paris Diderot, Sorbonne Paris Cité, CNRS, F-91191 Gif-sur-Yvette, France

2, Dipartimento di Fisica e Astronomia G. Galilei, Università di Padova, Vicolo dell'Osservatorio 3, 35122, Italy

3, Subaru Telescope, National Astronomical Observatory of Japan, National Institutes of Natural Sciences (NINS), 650 North A'ohoku Place, Hilo, HI, 96720, USA

4, Department of Astronomical Science, SOKENDAI (The Graduate University for Advanced Studies), 650 North A'ohoku Place, Hilo, HI, 96720, USA

5, Instituto de Física, Pontificia Universidad Católica de Valparaíso, Casilla 4059, Valparaíso, Chile

6, Key Laboratory of Modern Astronomy and Astrophysics in Ministry of Education, School of Astronomy and Space Science, Nanjing University, Nanjing 210093, China

7, Max Planck Institute for Astronomy, Königstuhl 17, D-69117 Heidelberg, Germany

8, Cavendish Laboratory, University of Cambridge, 19 JJ Thomson Avenue, Cambridge, CB3 0HE, UK.

9, Kavli Institute for Cosmology, University of Cambridge, Madingley Road, Cambridge CB3 0HA, UK

10, Astronomy Program, Department of Physics and Astronomy, Seoul National University, 599 Gwanak-ro, Gwanak-gu, Seoul, 151-742, Korea

11, Centro de Astronomía (CITEVA), Universidad de Antofagasta, Avenida Angamos 601, Antofagasta, Chile

12, Instituto de Física y Astronomía, Facultad de Ciencias, Universidad de Valparaíso, Gran Bretaña 1111, Playa Ancha, Valparaíso, Chile

13, National Optical Astronomy Observatory, 950 N. Cherry Avenue, Tucson, AZ 85719, USA

14, INAF-Osservatorio Astrofisico di Arcetri, Largo Enrico Fermi 5, 50125 Firenze, Italy

15, Dawn Cosmic Center, Niels Bohr Institute, University of Copenhagen Juliane Maries Vej 30, DK-2100 Copenhagen, Denmark

16, Dark Cosmology Centre, Niels Bohr Institute, University of Copenhagen, Juliane Maries Vej 30, DK-2100 Copenhagen, Denmark

17, European Southern Observatory, Karl Schwarzschild Straße 2, 85748 Garching, Germany

Accepted for publication in *ApJ Letters* July 13, 2018

ABSTRACT

We obtained optical/near-IR rest-frame Magellan FIRE spectra (including Pa β and Pa γ) of 25 starburst galaxies at $0.5 < z < 0.9$, with average star formation rates (SFR) $\times 7$ above the Main Sequence (MS). We find that Paschen-to-Balmer line ratios saturate around a constant value corresponding to $A_V \sim 2\text{--}3$ mag, while line to IR luminosity ratios suggest a large range of more extreme obscurations and appear to be uncorrelated to the former. This behavior is not consistent with standard attenuation laws derived for local and distant galaxies, while being remarkably consistent with observations of starburst cores in which young stars and dust are homogeneously mixed. This model implies $A_V = 2\text{--}30$ mag attenuation to the center of starburst cores, with a median of ~ 9 mag (a factor of 4000). X-ray hardness ratios for 6 AGNs in our sample and column densities derived from observed dust masses and radio sizes independently confirm this level of attenuation. In these conditions observed optical/near-IR emission comes from surface regions, while inner starburst cores are invisible. We thus attribute the high [NII]/H α ratios to widespread shocks from accretion, turbulence and dynamic disturbances rather than to AGNs. The large range of optical depths demonstrates that substantial diversity is present within the starburst population, possibly connected to different merger phases or progenitor properties. The majority of our targets are, in fact, morphologically classified as mergers. We argue that the extreme obscuration provides in itself smoking gun evidence of their merger origin, and a powerful tool for identifying mergers at even higher redshifts.

Keywords: galaxies: evolution — galaxies: starburst — galaxies: ISM — galaxies: high-redshift — infrared: galaxies

1. INTRODUCTION

Starburst galaxies (SBs) outliers from the MS (e.g., Noeske et al. 2007; Daddi et al. 2007), might be key to understand a long-standing mystery in galaxy formation and evolution: the transition from star forming galaxies to massive, passively evolving ellipticals. According to a popular scenario (e.g., Di Matteo et al. 2005; Hopkins et al. 2010), this transition is attributed to major mergers producing strong bursts of star formation in very dense cores and triggering obscured black hole accretion, which can both remove the gas and dust content in the galaxy.

Local ultra-luminous infrared galaxies (ULIRGs) are showcase examples of merger-induced starbursts, show-

ing compact and heavily obscured cores (e.g., Soifer et al. 2000; Juneau et al. 2009), in agreement with the above scenario. Using standard attenuation recipes in ULIRGs (Cardelli et al. 1989; Calzetti et al. 2000) leads to UV, optical and near-IR based SFRs being systematically underestimated compared to the total infrared luminosities, implying optically thick conditions for these tracers (Goldader et al. 2002; García-Marín et al. 2009; Rieke et al. 2009).

The nature and evolution of SBs galaxies in the distant Universe is debated. While they might still be major merger events, there are also claims that they might be instead very gas rich galaxies (e.g., Scoville et al. 2016),

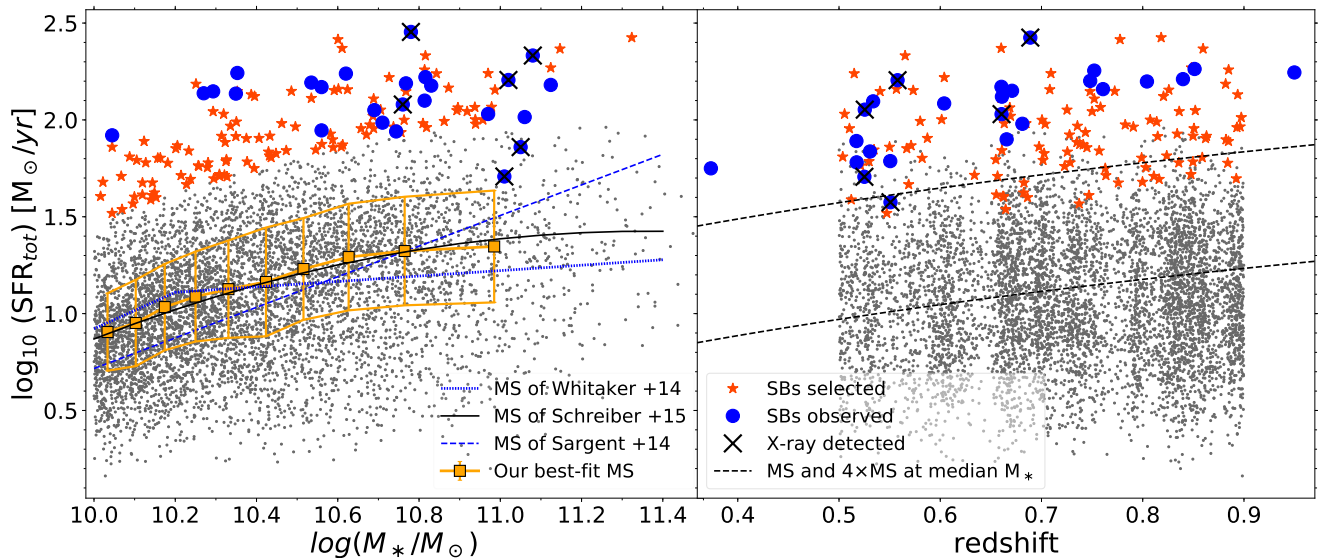


Figure 1. *Left:* SFR- M_* diagram for galaxies in our parent sample ($0.5 < z < 0.9$), where SFR_{tot} is defined as $SFR_{UV,obs} + SFR_{IR}$, and is normalized to their median redshift (0.73) using the evolving trend from Sargent et al. (2014). For sources detected only at $24\mu m$ we estimated the SFR from their $24\mu m$ flux using M12 templates. *Right:* SFR_{tot} vs redshift for the same sample.

possibly due to exceptionally strong gas accretion events. This is supported by ideas that at higher redshifts, with higher gas fractions, major mergers might only rarely result in strong SFR enhancements (Fensch et al. 2017). Comparisons of both dust-free and dust-affected SFRs are required to study their degree of obscuration, providing clues on the ULIRGs/distant-SB connection. Puglisi et al. (2017) showed that on average Balmer emission lines of Herschel-selected $z \sim 1.6$ SBs are mainly coming from regions producing $< 10\%$ of the total SFR, suggesting that rest-optical lines cannot be used to infer the physical properties of the whole starburst system. These results prompted us to use Magellan FIRE to obtain spectroscopy of starbursts in the near-IR rest-frame with the aim of providing enhanced sensitivity and constraining power to study their attenuation properties (hence their nature). In this letter we present first results of this effort. We adopt Chabrier (2003) IMF, AB magnitudes and standard cosmology ($H_0 = 70 \text{ km s}^{-1} \text{ Mpc}^{-1}$, $\Omega_m = 0.3$, $\Omega_\Lambda = 0.7$).

2. SAMPLE SELECTION

We select starburst galaxies for observations with Magellan FIRE in the COSMOS field, with the following criteria:

- spectroscopic redshift $0.5 < z < 0.9^1$ (from optical surveys, Salvato et al. in preparation), placing $Pa\beta$ within the K band, and $H\alpha$ above $0.82\mu m$, thus observable with FIRE².
- $SFR > 4 \times SFR_{MS}$ (Rodighiero et al. 2011)³. SFRs are

¹ We also added four galaxies with photometric redshifts (Laigle et al. 2016) lying in the same range.

² Existing spectroscopic redshift were incorrect for two galaxies, new redshifts placing them outside of our selection range (Fig. 1-right). We keep them in the sample as they satisfy the other selection criteria.

³ Because of the unavoidable variations of the IR photometry

derived using the IR catalog from Jin et al. (2018)⁴. As shown in Fig. 1, the MS for our sample, derived through a running median over 10 bins in M_* , agrees with the literature (Sargent et al. 2014; Schreiber et al. 2015). Our SFRs are de-contaminated from AGN torus emission (3% median contribution to L_{IR} ; see Liu et al. (2018) and Jin et al. (2018) for the procedure).

- $M_* > 10^{10} M_\odot$, for sample completeness: above this mass limit and up to $z = 0.9$, all SBs would be Herschel detected at $S/N_{FIR} > 5$ (cf. Fig. 16 in Jin et al. (2018)). Stellar masses are from Laigle et al. (2016).

These criteria yield a total of 152 starburst candidates for our Magellan observations (Fig. 1). They represent 2-3% of the whole star-forming population in the same mass range and redshift, (see, e.g., Sargent et al. 2012, 2014; Schreiber et al. 2015).

3. MAGELLAN-FIRE OBSERVATIONS

FIRE is a single slit near-infrared spectrometer mounted at the Magellan 6.5m Baade Telescope, covering the wavelength range $0.82\text{--}2.4\mu m$. We observed in the cross-dispersed echelle mode, choosing a slit width of $1''$ to maximize the incoming light from our targets. This configuration provides a spectral resolution $R \simeq 3000$, which helps reducing the effect of OH sky-emission. We refer to Simcoe et al. (2013) for a complete description of the instrument and its performances.

among different catalog versions, while they were being built, two objects appear now slightly below this $\times 4$ threshold (Fig. 1-left).

⁴ Accurate SFR measurements were derived by fitting IRAC to radio 20cm photometry from Jin et al. (2018) with four components as follows: a Bruzual & Charlot (2003) SED for the stellar component (with age 200 Myr, constant SFH, Z_\odot , Chabrier IMF and Calzetti attenuation law), a mid-infrared AGN template from Mullaney et al. (2011) and a warm+cold dust SED from the full Draine & Li (2007) library.

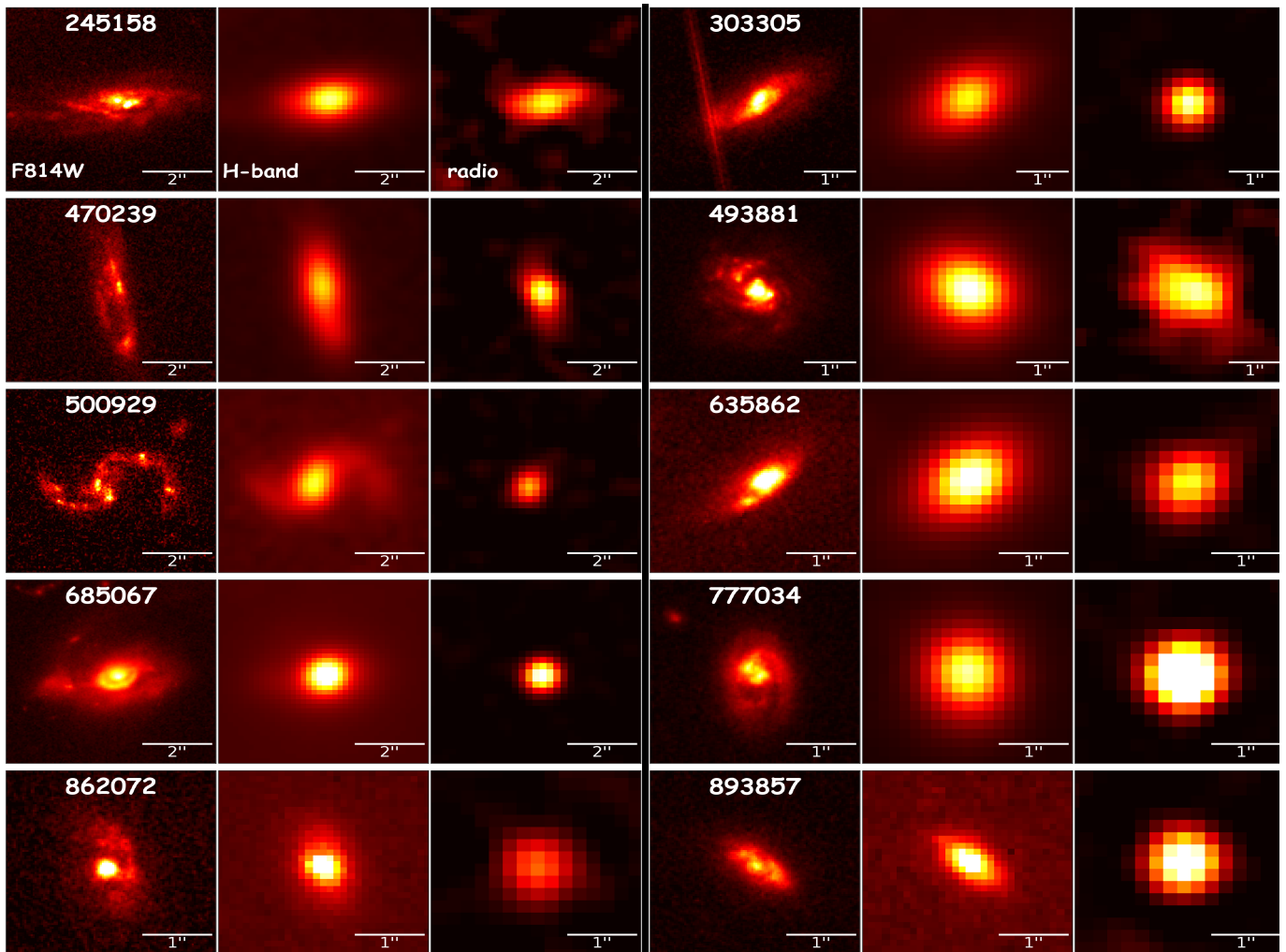


Figure 2. *Left:* HST-ACS F814W cutout images for 10 galaxies of our Magellan sample. Their FWHM resolution is $0.095''$. *Center:* H-band UltraVISTA images with the same f.o.v. and with $\text{FWHM}_{\text{res}} \sim 0.75''$. *Right:* 3 GHz radio images from VLA-COSMOS 3GHz Large Project (Smolčić et al. 2017), $\text{FWHM} \sim 0.75''$. For the galaxies 862072 and 893857, higher resolution ($0.2''$) H-band cutouts from the COSMOS-DASH program are shown (Momcheva et al. 2016).

Our observations were performed in two runs during the nights of 17-18 March 2017 and 22-23 March 2018. We prioritized targets for observations based on two criteria: (1) the presence of a nearby ($\lesssim 30''$ from the target) bright ($J < 19$ -20 mag) star to facilitate acquisition, and (2) maximization of the ratio $\text{SFR}_{\text{IR}}/D_L^2(z)$, where D_L is the luminosity distance. The latter condition select galaxies with intrinsically brightest emission lines, and tend to bias our observed sample towards the most massive objects (Fig. 1). We observed 11 targets during the first run and 14 in the second, for a total of 25 starbursts. Integration times ranged between 30 and 80 minutes, longer for galaxies with lower $\text{H}\alpha$ S/N (from real-time reductions), to improve detection of fainter lines.

The spectra were reduced using the FIRE pipeline (Gagné et al. 2015). Full details will be given in a forthcoming paper (Calabrò et al. in prep), also presenting science results for the complete range of observed emission lines. In Fig. 3, we show examples of $\text{H}\alpha$ and $\text{Pa}\beta$ (or $\text{Pa}\gamma$) for some of the galaxies with good detection ($\text{S/N} > 5$) of both lines. Double Gaussian components were fitted to line profiles whenever single Gaussian fits could be rejected based on χ^2 statistics, resulting always

in good fits ($\chi^2_{\text{red}} < 1.5$). We attribute these double Gaussians to either rotation or the presence of physically separated components.

The target list with main physical properties are presented in Table 1, while i-band, H-band and radio (3 GHz) cutout images of representative targets are shown in Fig. 2.

4. RESULTS

The wide spectral coverage of FIRE and the wealth of photometric data available for our targets makes this a unique sample to investigate attenuation through the use of different indicators as emission lines and the total infrared luminosity. In Fig. 4-left⁵ we compare the ratio of $\text{H}\alpha$ and $\text{Pa}\beta$ (Paschen-Balmer decrement) to the ratio of SFRs derived from the observed $\text{Pa}\beta$ and bolometric IR ($A_{\text{Pa}\beta, \text{IRX}} = 2.5 \times \log_{10}(1 + \text{SFR}_{\text{IR}}/\text{SFR}_{\text{Pa}\beta, \text{obs}})$ ⁶, where $\text{SFR}_{\text{Pa}\beta, \text{obs}}$ has been derived from the observed $\text{Pa}\beta$ lu-

⁵ This plot is equivalent to an IRX- β plot (Meurer et al. 1999).

⁶ For three galaxies in our sample where $\text{Pa}\beta$ falls in nearly opaque atmospheric spectral regions or out of FIRE coverage, we use $\text{Pa}\gamma$ line to infer the attenuation, estimating $\text{Pa}\beta$ flux as $2.2 \times \text{Pa}\gamma$ (Table 1). Indeed, both in a mixed model and foreground

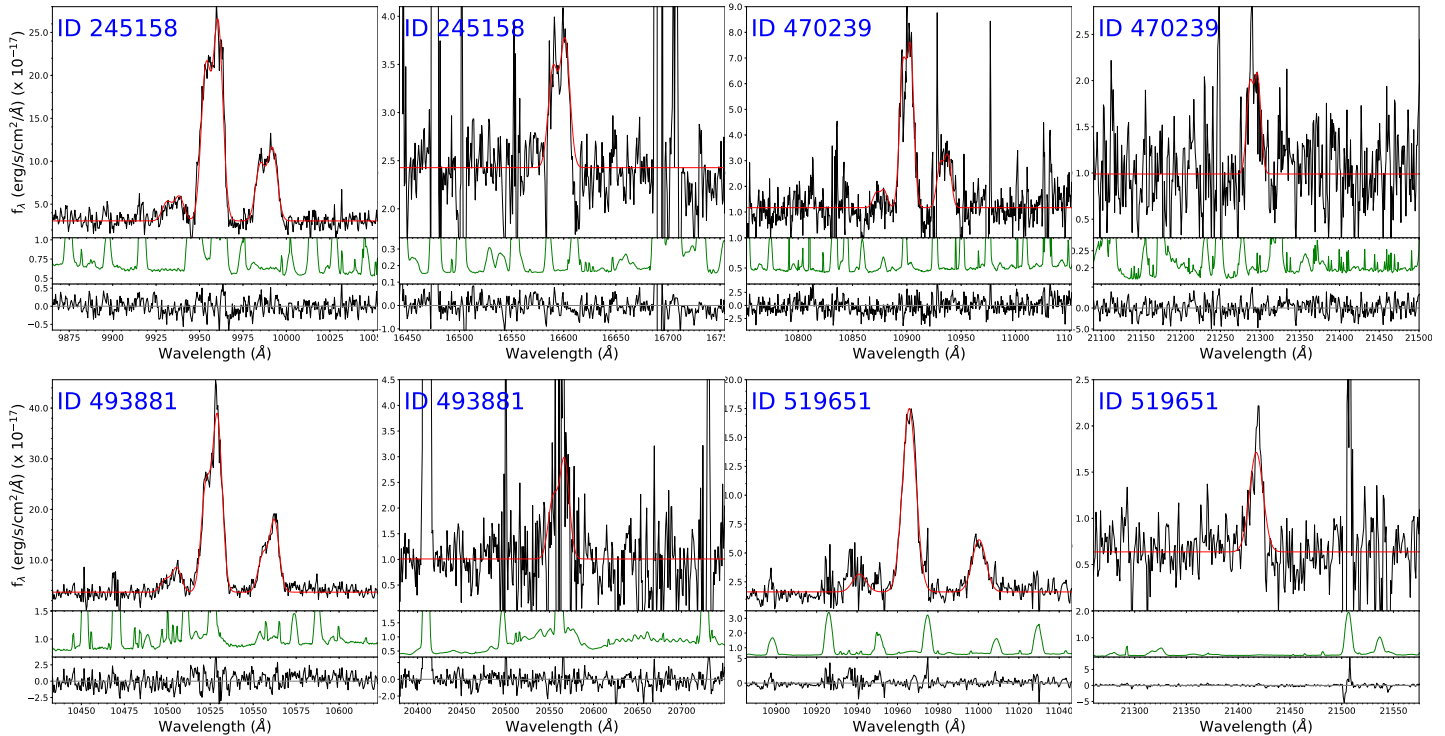


Figure 3. $H\alpha$ and $Pa\beta$ ($Pa\gamma$ for ID 245158) emission lines for 4 representative galaxies. In each panel, the spectra around the lines are shown, together with their best-fit gaussians in red, derived with MPFIT (Markwardt 2009). In the bottom panels we display the noise and the residual of the fit (data-model) normalized by the noise.

minosity, adopting an intrinsic ratio $Pa\beta/H\alpha = 0.057$ and a standard Kennicutt et al. (1994) calibration, valid for case B recombination and $T_e = 10^4 K$. We show that for our 25 starbursts, these two ratios, both independent measures of attenuation, do not generally scale as predicted by the Calzetti et al. (2000) and Cardelli et al. (1989) attenuation curves⁷. The value of $Pa\beta/H\alpha$ rather saturates at ~ 0.18 (with a dispersion of ~ 0.08 dex), qualitatively consistent with an optically thick ‘mixed model’, in which different lines probe different optical depths.

As opposed to the foreground dust-screen, a mixed model is made of a uniform extended distribution of young stars and dust inside a volume. In the one-dimensional case, a simple analytic relation can be derived between the observed and intrinsic SFR by integrating along a segment the luminosity contribution from each differential volume element, subject to the extinction of the full optical depth in front of it. This yields:

$$\frac{SFR_{obs}(\lambda)}{SFR_{intr}(\lambda)} = \frac{L(\lambda)_{obs}}{L(\lambda)_{intr}} = \frac{\log_{10}(e)}{0.4} \times \left(\frac{1 - 10^{-0.8A_{tot}(\lambda)}}{2A_{tot}(\lambda)} \right) \quad (1)$$

where $L(\lambda)$ is the luminosity of a line at a wavelength λ and $A_{tot}(\lambda)$ is the total absolute attenuation at λ towards the center defined as $k(\lambda)A_{V,tot}/R_V$. In the last expression, $k(\lambda)$ and R_V correspond to the local extinction, for which we assumed two extreme cases of a Cardelli et al. (1989) and an SMC (Bouchet et al. 1985) law, yielding an asymptotic $Pa\beta/H\alpha$ ratio of 0.17 and 0.2, respectively.

dust-screen geometry, the expected observed ratio $Pa\beta/Pa\gamma$ ranges between 2.1 and 2.3, for all the attenuation values in our range.

⁷ The Cardelli relation is actually an extinction law.

Using equation 1⁸, we can predict the observed fluxes at all wavelengths as a function of a single parameter, $A_{V,tot}$. For small values of $A_{V,tot}$ this model coincides with the standard attenuation curves adopted. For large $A_{V,tot}$, the local extinction inside the starburst core increases toward the center until the photons are not able to escape anymore from the galaxy, and are fully absorbed by the outer layers of dust. This leads us to depict heavily obscured starbursts as made of a central optically thick core, invisible to us, and a surrounding *skin*, producing the observed optical and near-IR nebular lines.

This picture naturally explains both the larger attenuation and SFR fraction that can be recovered by near-IR observations with respect to optical studies (Puglisi et al. 2017), as near-IR wavelengths allow us to penetrate deeper in the system. Because only the less attenuated light from the skin comes out, from $Pa\beta$ we can recover, on average, 30% of the total IR SFR (Fig. 4-middle). However, inside the skin the optical depth becomes quickly large, with median $A_{V,tot, mixed model} = 9$, corresponding to a suppression of $\times 4000$ of V-band light from the starburst core centers and up to extreme cases with $A_{V,tot, mixed model} \sim 30$ (10^{12} in linear scale). Hence, we cannot directly see the starburst cores in the optical/near-IR.

5. DISCUSSION

Can we conclude that $z \sim 0.7$ SBs contain extremely obscured cores that are well described by mixed stars/dust models? It is worth considering alternative explanations. It might be possible that the UV radi-

⁸ Calzetti et al. (1994) derived a similar equation (n.19) for a mixing geometry

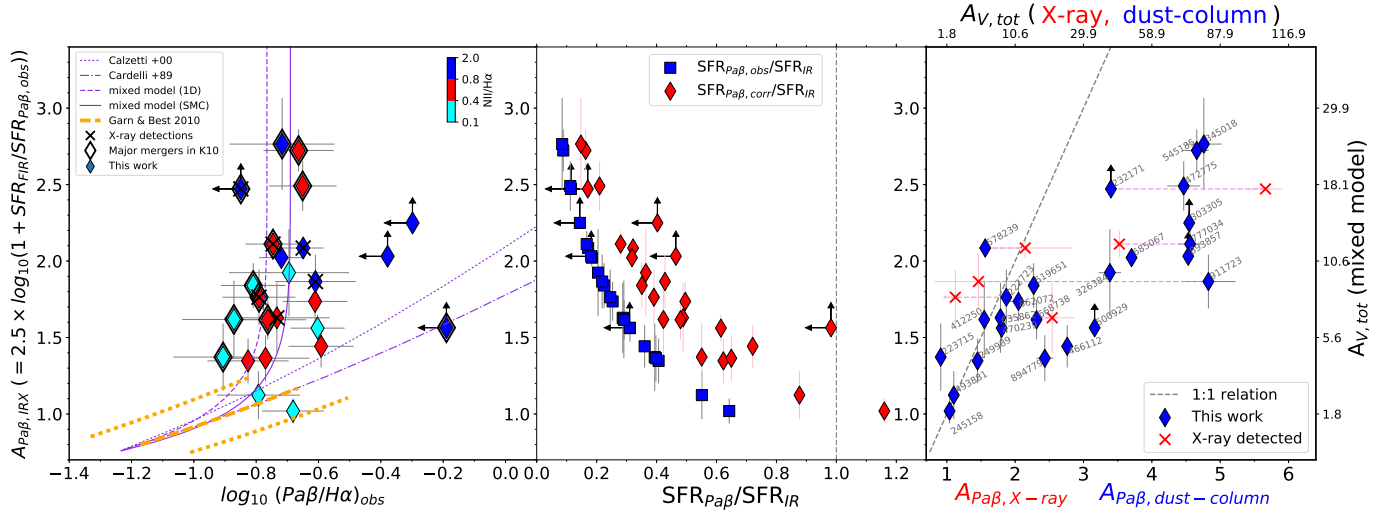


Figure 4. *Left:* Diagram comparing the observed $Pa\beta/H\alpha$ ratio and $A_{Pa\beta,IRX}$. Upper and lower limits are shown with arrows for four galaxies in the sample, while a color coding highlights their $[N II]/H\alpha$ values. *Center:* Ratio of the SFR (relative to IR) derived from the observed $Pa\beta$ line (blue) and after correcting the $Pa\beta$ fluxes using the Balmer($H\alpha$)-Paschen(β) decrement and a Calzetti et al. (2000) attenuation law (red). We remark that the unobscured UV SFR represents $\sim 1\%$ of that derived from the IR, thus its contribution to the total SFR is negligible for our sample. *Right:* Comparison between $A_{Pa\beta,IRX}$, which directly translates into the total A_V towards the center of a mixed model (right axis) with: (blue circles) $A_{Pa\beta}$ derived from the dust column-density and (red crosses) $A_{Pa\beta}$ calculated from X-ray hydrogen column-density N_H (Lanzuisi et al. 2017) for X-ray detected galaxies, as explained in the text.

tion from newly born massive stars is absorbed by dust within HII regions, before reaching to ionize HI outside. While strong stellar winds push the dust away to form a screen (Calzetti et al. 2000), a substantial amount of absorbing dust may still be trapped in the ongoing SF site (Caplan & Deharveng 1986; Bell & Kennicutt 2001) particularly in these very dust rich galaxies. This would simulate the existence of an optically thick SB core, just reducing the fraction of photons seen by HI. This could still represent a mixed model scenario, with mixing occurring at smaller scales. Whether this is a viable option depends on geometry and is difficult to model in detail.

Alternatively, the discrepant SFRs (coming from the lines and IR bolometric luminosity) may be due to time-variation effects, as L_{IR} probes longer SFR timescales than emission lines, due to the energy contribution of longer-lived B-type stars to ionizing O stars. In our case, this would require that most SBs have recently experienced a severe SFR truncation, which seems unlikely. Instantaneous and dust-free SFR tracers, like e.g., through CO[5-4] lines (Daddi et al. 2015), would shed light and help addressing definitely this possibility.

Due to the optically thick cores, the mixed model also implies that it might not be possible to detect AGNs from optical and near-IR observations, if located in the coalescing center. Interestingly, Fig. 4 shows that our SB galaxies often display high $N2$ ($\equiv \log[N II]/H\alpha$) indexes, which might suggest highly ionizing, AGN-dominated emission. We also see a correlation, significant at $> 95\%$ confidence level (Spearman correlation coefficient $r = 0.5$), between $N2$ and $A_{V,tot, mixed model}$ ⁹. We argue that instead, in the majority of our targets with enhanced $[N II]/H\alpha$ (and relatively higher obscurations), the line emission may be driven by shocks, which were already

shown to contribute up to 50% in local ULIRGs in latest merger stages (Rich et al. 2015). In case of shock contribution, the attenuations that we have inferred through $A_{Pa\beta,IRX}$ would represent lower limits, but the line ratios will not be affected as Case B recombination regime still holds.

Nevertheless, it would be crucial to obtain independent estimates of actual attenuations towards the cores. One possibility is provided by AGNs. We searched for evidence of AGNs among our SBs using multiple dust-free multi-wavelength tracers in the radio and X-rays. While none of our SBs show significant radio excess, either following the criteria of Del Moro et al. (2013) and the less stringent requirements of Liu et al. (2018) (all assuming an IR-radio correlation), six galaxies (ID 578239, 635862, 777034, 232171, 222723, and 911723) are detected by XMM-Newton, Chandra or NuStar (Cappelluti et al. 2009; Marchesi et al. 2016; Civano et al. 2015) with luminosities much higher than what expected from their SFRs (Ranalli et al. 2004). The same objects are also the only ones in which we detect a mid-IR dusty torus component through SED fitting (only tentative for SB 578239). Their X-ray hardness ratios were converted in obscuring column densities (N_H) by Lanzuisi et al. (2017; see Fig.19 in La Massa et al 2016 for the method), which are N_H upper limits for gas/dust obscurations to the cores (part of the obscuration would happen within the torus itself). The relation of Güver & Özel (2009) allows to convert N_H into a total A_V and ($N_H(\text{cm}^2) = 2.21 \times 10^{21} A_V(\text{mag})$). This returns generally very high X-ray obscurations for the AGNs (Fig. 4-right), supporting the presence of high obscuration in their center, as required by the mixed model.

As a further check, we computed the column density of gas in the starbursts cores using the total molecular mass M_{mol} , inferred as $M_{mol} = 8.05 + 0.81 \times \log(SFR)$ (Sargent

⁹ This incidentally suggests that the four galaxies with $Pa\beta$ upper limits are also very highly obscured, having relatively high $N2$.

et al. 2014, , assuming conservatively the starburst case) and the radio size, measured with GALFIT by fitting a gaussian profile (convolved with the PSF) to their VLA (3 GHz) images (Fig. 2). From Fig. 4-right we can see that for half of our sample, at relatively low-moderate obscurations within the probed range, the attenuation inferred from this method is consistent with the mixed model. On the other hand, towards the highest obscurations, this approach suggests even larger attenuations. Some fraction of the emission line fluxes might come from foreground regions unrelated to the starbursting cores, presumably residual material from the merging galaxies. Accounting for this extra, modestly attenuated component would result in substantial increase of the $A_{V,tot}$ of the starburst core, providing better agreement with these column densities estimates. A proper correction for this effect would require IFU observations, that could also clarify whether our objects are similar to local ULIRGs, for which higher values of nuclear attenuations ($A_V \sim 10$ -1000 mag) are reported in several studies (e.g., Scoville et al. 1998; Genzel et al. 1998). All in all, it appears that very heavily embedded cores are indeed present in these galaxies.

What is the origin of these extremely obscured cores? Unsurprisingly (Fig. 2), morphological classification was independently derived for 18 starbursts in our sample (Kartaltepe et al. 2010, see Tab. 1), and over 83% of them were identified as mergers: 11 as major mergers (61%), showing distorted or double nuclei, tidal tails, bridges or overlapping disks, and 4 (22%) as minor mergers, characterized by at least slightly disturbed morphology (e.g., warped disks, asymmetric spiral arms, small companion at same z , etc). Visual inspection for the remaining sources suggest that merger origin is at least plausible for the vast majority of our sample. Mergers are, in fact, more commonly identified among less obscured systems (Tab. 1), which is understandable given that in the later coalescence phases any remaining merger signature becomes subtle (see, e.g., two of the three morphologically non-merger objects in our sample classified as Ellipticals/S0 by Kartaltepe et al. (2010), and the three of them have $A_{V,tot} > 9$). It is thus tempting to attribute the large range of observed properties apparently defining a sequence of obscurations as reflecting different merger phases, to varying progenitor properties (including, e.g., the gas fraction of merging galaxies and the impact geometry), or a combination of them. Nevertheless, we cannot definitely exclude with our data that the sequence may be also reflecting the amount of foreground contamination, thus unrelated to the real obscuration of the core.

Our work suggests that deeply embedded merger events still largely dominate among sample of SBs galaxies at least to $z \sim 0.7$, which corresponds to 6.3 Gyr lookback time, an epoch with galaxy specific SFRs $> 5\times$ larger than local on average. At even higher redshifts, it becomes much harder to identify mergers from their morphological signatures due to surface brightness dimming and widespread presence of clumpy/irregular galaxies. We argue instead that higher- z mergers might be even more efficiently identified searching for evidences of extreme levels of obscurations, given our results and also consistently with simulations (e.g. Di Matteo et al. 2005), representing a clear footprint of their origin. In fact, we

are not aware of any viable alternative mechanism that could produce galaxy-wide obscurations of 10+ mag in the V-band: normal disk-like galaxies display much lower obscurations (orange lines in Fig.4-left). Near-IR rest-frame spectra of galaxies will be easily accessible soon with JWST up to $z \simeq 7$ and down to much fainter levels, and will allow testing and applying this idea.

We thank the referee for useful suggestions, G. Rudie for assistance with Magellan observations, Nicolás Ignacio Godoy for data reduction, and Daniela Calzetti for discussions. We acknowledge support from FONDECYT regular programs 1150216 and 1170618, by the Brain Pool Program, funded by the Ministry of Science and ICT through the Korean National Research Foundation, and RadioNet conference funding (2018H1D3A2000902).

REFERENCES

- Bell, E. F., & Kennicutt, R. C., Jr. 2001, *ApJ*, 548, 681
 Bouchet, P., Lequeux, J., Maurice, E., Prevot, L., & Prevot-Burnichon, M. L. 1985, *A&A*, 149, 330
 Bruzual, G., & Charlot, S. 2003, *MNRAS*, 344, 1000
 Calzetti, D., Armus, L., Bohlin, R. C., et al. 2000, *ApJ*, 533, 682
 Calzetti, D., Kinney, A. L., & Storchi-Bergmann, T. 1994, *ApJ*, 429, 582
 Caplan, J., & Deharveng, L. 1986, *A&A*, 155, 297
 Cappelluti, N., Brusa, M., Hasinger, G., et al. 2009, *A&A*, 497, 635
 Cardelli, J. A., Clayton, G. C., & Mathis, J. S. 1989, *ApJ*, 345, 245
 Chabrier, G. 2003, *PASP*, 115, 763
 Civano, F., Hickox, R. C., Puccetti, S., et al. 2015, *ApJ*, 808, 185
 Daddi, E., Dickinson, M., Morrison, G., et al. 2007, *ApJ*, 670, 156
 Daddi, E., Dannerbauer, H., Liu, D., et al. 2015, *A&A*, 577, A46
 Del Moro, A., Alexander, D. M., Mullaney, J. R., et al. 2013, *A&A*, 549, A59
 Di Matteo, T., Springel, V., & Hernquist, L. 2005, *Nature*, 433, 604
 Draine, B. T., & Li, A. 2007, *ApJ*, 657, 810
 Fensch, J., Renaud, F., Bournaud, F., et al. 2017, *MNRAS*, 465, 1934
 Güver, T., & Özel, F. 2009, *MNRAS*, 400, 2050
 Jonathan Gagné, Erini Lambrides, Jacqueline K. Faherty, Robert Simcoe. FireHose.v2: Firehose v2.0. Zenodo ; 2015
 García-Marín, M., Colina, L., & Arribas, S. 2009, *A&A*, 505, 1017
 Garn, T., & Best, P. N. 2010, *MNRAS*, 409, 421
 Genzel, R., Lutz, D., Sturm, E., et al. 1998, *ApJ*, 498, 579
 Goldader, J. D., Meurer, G., Heckman, T. M., et al. 2002, *ApJ*, 568, 651
 Hopkins, P. F., Bundy, K., Croton, D., et al. 2010, *ApJ*, 715, 202
 Jin, S., Daddi, E., et al. 2018, submitted to *ApJ*
 Juneau, S., Narayanan, D. T., Moustakas, J., et al. 2009, *ApJ*, 707, 1217
 Kartaltepe, J. S., Sanders, D. B., Le Floc'h, E., et al. 2010, *ApJ*, 721, 98
 Kennicutt, R. C., Jr., Tamblyn, P., & Congdon, C. E. 1994, *ApJ*, 435, 22
 Laigle, C., McCracken, H. J., Ilbert, O., et al. 2016, *ApJS*, 224, 24
 LaMassa, S. M., Civano, F., Brusa, M., et al. 2016, *ApJ*, 818, 88
 Lanzuisi, G., Delvecchio, I., Berta, S., et al. 2017, *A&A*, 602, A123
 Liu, D., Daddi, E., Dickinson, M., et al. 2018, *ApJ*, 853, 172
 Marchesi, S., Lanzuisi, G., Civano, F., et al. 2016, *ApJ*, 830, 100
 Markwardt, C. B. 2009, *Astronomical Data Analysis Software and Systems XVIII*, 411, 251
 Meurer, G. R., Heckman, T. M., Calzetti, D., 1999, *ApJ*, 521, 64
 Momcheva, I. G., Brammer, G. B., van Dokkum, P. G., et al. 2016, *ApJS*, 225, 27
 Mullaney, J. R., Alexander, D. M., Goulding, A. D., & Hickox, R. C. 2011, *MNRAS*, 414, 1082
 Noeske, K. G., Weiner, B. J., Faber, S. M., et al. 2007, *ApJL*, 660, L43

Table 1
Main properties of the Magellan starbursts

ID	RA (deg)	DEC (deg)	z_{spec}	$\log(M_*)$ (M_\odot)	$\log(\text{LIR}_{\text{SFR}})$ (L_\odot)	$\text{H}\alpha$ ($10^{-17} \frac{\text{erg}}{\text{cm}^2}$)	$\text{Pa}\beta$ ($10^{-17} \frac{\text{erg}}{\text{cm}^2}$)	$A_{V,\text{tot}}$ (mag)	$N_{\text{H,X}}$ (cm^{-2})	M_{type}
245158	150.18854	1.65498	0.5172	10.7	11.89 ± 0.07	249.6 ± 30.1	$52.0 \pm 5.6^\ddagger$	1.9 ± 0.1	-	S,m
493881	150.74967	2.04707	0.6039	10.8	12.09 ± 0.06	330.9 ± 30.2	53.3 ± 11.5	2.7 ± 0.2	-	-
223715	149.76537	1.61702	0.5174	10.7	11.78 ± 0.03	204.0 ± 20.8	28.5 ± 6.6	3.6 ± 0.2	-	m,S
249989	150.68540	1.66108	0.6656	10.6	11.90 ± 0.08	127.6 ± 15.9	19.0 ± 3.3	4.4 ± 0.2	-	MIII
894779	150.42710	2.65644	0.5506	10.0	11.79 ± 0.03	129.7 ± 19.3	22.0 ± 3.8	4.5 ± 0.2	-	MIV
466112	149.99928	2.00599	0.7607	10.3	12.16 ± 0.04	81.7 ± 6.2	20.9 ± 3.5	5.2 ± 0.3	-	MIII
470239	150.48155	2.01096	0.6609	10.6	12.12 ± 0.17	92.3 ± 9.5	23.0 ± 2.2	6.2 ± 0.2	-	-
500929	149.76844	2.05935	0.9498	10.8	12.25 ± 0.14	21.9 ± 5.3	$< 14.3^\ddagger$	> 6.2	-	MIII
412250	150.74171	1.91764	0.8397	10.3	12.21 ± 0.04	118.6 ± 10.5	16.0 ± 4.7	6.7 ± 0.6	-	MIII
668738	150.21020	2.31168	0.7481	10.8	12.20 ± 0.04	81.4 ± 7.5	14.1 ± 1.4	6.7 ± 0.2	-	MIII
635862	149.69589	2.26450	0.5508	11.0	11.58 ± 0.10	59.7 ± 8.8	11.0 ± 2.7	6.8 ± 0.6	22.54 ± 0.14	-
862072	150.12329	2.60376	0.6811	11.1	11.98 ± 0.07	58.3 ± 6.0	14.3 ± 1.9	7.8 ± 0.4	-	m,S
222723	150.17321	1.61632	0.5254	11.0	12.05 ± 0.05	150.7 ± 11.1	24.4 ± 4.8	8.1 ± 0.5	< 21.66	MV
519651	150.43020	2.08688	0.6709	10.5	12.15 ± 0.05	126.0 ± 10.5	19.5 ± 3.0	8.8 ± 0.5	-	MIV
911723	149.68134	2.68108	0.6606	10.8	12.03 ± 0.02	65.9 ± 7.2	16.2 ± 3.1	9.1 ± 0.6	21.98 ± 0.36	E
326384	149.51786	1.78357	0.8042	10.3	12.20 ± 0.07	68.8 ± 8.8	12.4 ± 3.8	9.8 ± 1.1	-	S
685067	149.74730	2.34574	0.3735	11.0	11.75 ± 0.01	136.9 ± 16.5	26.1 ± 1.2	10.9 ± 0.3	-	-
893857	150.15995	2.65434	0.8512	11.1	12.26 ± 0.09	27.4 ± 1.6	$< 11.5^\ddagger$	> 11	-	E
578239	150.76543	2.18099	0.5578	11.1	12.21 ± 0.23	116.5 ± 10.4	26.1 ± 1.6	11.7 ± 0.3	22.36 ± 0.31	-
777034	150.15025	2.47517	0.6889	10.8	12.43 ± 0.08	114.0 ± 13.3	20.5 ± 1.8	12.0 ± 0.4	22.96 ± 0.04	MIV
303305	150.48305	1.74796	0.5306	10.7	11.84 ± 0.10	19.9 ± 3.6	$< 10.0^\ddagger$	> 13.9	-	-
232171	150.06033	1.63269	0.5251	11.1	11.71 ± 0.02	60.1 ± 14.2	< 8.5	> 17.6	23.83 ± 0.1	MII
472775	150.48148	2.01362	0.6604	10.8	12.17 ± 0.06	44.3 ± 4.1	9.9 ± 1.6	18.0 ± 1.3	-	-
545185	149.52802	2.12725	0.5337	10.4	12.10 ± 0.06	49.8 ± 4.2	10.9 ± 0.9	22.5 ± 1.0	-	MIII
345018	149.72556	1.81069	0.7521	10.6	12.25 ± 0.06	37.0 ± 3.6	7.1 ± 2.1	23.7 ± 3.4	-	m,S

Note. ID, RA, DEC (J2000) and M_* are from [Laigle et al. \(2016\)](#). The $1-\sigma$ error on M_* is 0.1 dex. Line fluxes are measured from aperture corrected spectra. Aperture correction errors (~ 0.04 dex) are included in the uncertainties. The infrared luminosities (integrated between 8-1000 μm), are AGN-torus decontaminated. $\text{H}\alpha$ and $\text{Pa}\beta$ are corrected for stellar absorption, assuming $\text{EW}_{\text{abs}} = 2.6$ and 2 \AA , respectively. The morphological type (M_{type}) of [Kartaltepe et al. \(2010\)](#): E=Elliptical/S0; S=spiral/disc; m=Minor merger; M=Major merger (I:first approach, II:first contact, III:pre-merger, IV:Merger, V:Old merger/merger remnant). The galaxies are ordered with increasing $A_{V,\text{tot}}$. ‡ : derived as $\text{Pa}\beta = 2.2 \times \text{Pa}\gamma$

Puglisi, A., Daddi, E., Renzini, A., et al. 2017, *ApJL*, 838, L18
Ranalli, P., Comastri, A., & Setti, G. 2004, *Multiwavelength AGN Surveys*, 43
Rich, J. A., Kewley, L. J., & Dopita, M. A. 2015, *ApJS*, 221, 28
Rieke, G. H., Alonso-Herrero, A., Weiner, B. J., et al. 2009, *ApJ*, 692, 556
Rodighiero, G., Daddi, E., Baronchelli, I., et al. 2011, *ApJL*, 739, L40
Sargent, M. T., Béthermin, M., Daddi, E., & Elbaz, D. 2012, *ApJL*, 747, L31
Sargent, M. T., Daddi, E., Béthermin, M., et al. 2014, *ApJ*, 793, 19

Schreiber, C., Pannella, M., Elbaz, D., et al. 2015, *A&A*, 575, A74
Scoville, N. Z., Evans, A. S., Dinshaw, N., et al. 1998, *ApJL*, 492, L107
Scoville, N., Sheth, K., Aussel, H., et al. 2016, *ApJ*, 820, 83
Simcoe, R. A., Burgasser, A. J., Schechter, P. L., et al. 2013, *PASP*, 125, 270
Smolčić, V., Novak, M., Bondi, M., et al. 2017, *A&A*, 602, A1
Soifer, B. T., Neugebauer, G., Matthews, K., et al. 2000, *AJ*, 119, 509